



Scintillation and thermally stimulated luminescence properties of Ce-doped SrO–Al₂O₃–SiO₂ glasses

Hiromi Kimura¹ · Hirokazu Masai² · Takumi Kato¹ · Daisuke Nakauchi¹ · Noriaki Kawaguchi¹ · Takayuki Yanagida¹

Received: 16 October 2019 / Accepted: 30 December 2019 / Published online: 7 January 2020
© Springer Science+Business Media, LLC, part of Springer Nature 2020

Abstract

45SrO–5Al₂O₃–50SiO₂ glasses doped with various concentrations of Ce (0, 0.01, 0.05, 0.1, and 0.5 mol%) were synthesized by the conventional melt-quenching methods, and the basic optical, scintillation, and thermally stimulated luminescence (TSL) properties were investigated. Regarding the optical properties, under 340 nm excitation, the emission peak around 420 nm of the Ce-doped glasses was confirmed. The emission would be due to the 5d → 4f transitions of Ce³⁺. In contrast, the scintillation spectra of all the glasses showed two emission peaks around 350 and 400 nm, and the origins would be some defects or impurity ions included in the host glass. By ²⁴¹Am 5.5 MeV α-ray irradiation, the non-doped glass showed the highest light yield, which was 69 photons/MeV with a typical error of ± 10%. As the TSL properties, the TSL intensity of 0.01% Ce-doped glass was the highest among the prepared glasses, and a linear response to the irradiation dose was confirmed in the dose range of 0.01–1000 mGy.

1 Introduction

Ionizing radiation detectors using luminescent materials have been utilized in industrial and scientific fields such as medical imaging [1–3], security system [4], individual radiation monitoring [5], well logging [6], and astrophysics [7]. Such materials are mainly classified into two types of scintillators and storage phosphors. Scintillators convert the absorbed energy of ionizing radiation such as X-rays and γ-rays into many low-energy photons immediately. In contrast, storage phosphors store a part of the absorbed energy, and the stored energy is released by the stimulation of heat (Thermally stimulated luminescence, TSL) or light (Optically stimulated luminescence, OSL) to emit photons. These photons are converted to electrons by photodetectors such as photo-multiplier tube (PMT) and Si photodiode. Formerly, scintillators and storage phosphors were studied in different field, while they share common physical processes. In recent

years, it is pointed out that the light yield of scintillators and the emission (e.g., TSL or OSL) intensity of storage phosphors are complementarily related in some materials [8–12]. Therefore, it is important to investigate both the properties inclusively in one material.

So far, most of scintillation materials are designed as a combination of host matrix materials and emission center [13, 14]. The former absorbs the radiation energy, and the latter converts the absorbed energy to low-energy photons. The host matrix materials are required to have the suitable chemical composition for the radiation types such as high-energy photons, charged particles, and neutrons. When the target of detection is high-energy photons (e.g., γ-rays), the heavy materials are selected. In contrast, in the case of charged particles, the host matrix materials with medium effective atomic number (Z_{eff}) are preferred because the heavy materials have a high cross-section to background X- and γ-rays. If the target of detection is neutrons, the light material containing ⁶Li, ¹⁰B, or ¹⁵⁷Gd are selected since they have a high cross-section against thermal neutron. The emission center is required to have a function to efficiently emit photons, and rare earth ions are generally selected.

Conventionally, the forms of common scintillation materials have been used mainly bulk single crystals because they have high optical qualities. From the viewpoint of industry, the single crystals have some disadvantages including low mechanical strength and high cost, while the glasses resolve

✉ Hiromi Kimura
kimura.hiromi.kf1@ms.naist.jp

¹ Division of Materials Science, Nara Institute of Science and Technology (NAIST), 8916-5 Takayama-cho, Ikoma-shi, Nara 630-0192, Japan

² National Institute of Advanced Industrial Science and Technology (AIST), 1-8-31 Midorigaoka, Ikeda, Osaka 563-8577, Japan

these disadvantages [15–19]. Additionally, the glasses can be selected due to a flexibility of chemical composition in material designs. However, the practical scintillator in the form of glasses is only Li-glass (GS20, Saint-Gobain) for neutron detectors [20]. Therefore, there is room for researching glass materials in radiation detectors.

In this paper, to develop the new charged particle detectors in the form of glasses, we focus on $45\text{SrO}-5\text{Al}_2\text{O}_3-50\text{SiO}_2$ glass. The Z_{eff} of the glass ($Z_{\text{eff}} \sim 31.7$) is close to that of the practical scintillator for the charged particle detectors such as Eu-doped CaF_2 ($Z_{\text{eff}} \sim 17.1$) and Ag-doped ZnS ($Z_{\text{eff}} \sim 27.4$). In previous reports, Sm- or Mn-doped $\text{SrO}-\text{Al}_2\text{O}_3-\text{SiO}_2$ glasses have been studied as phosphors for white light emitting diode application [21, 22]. In addition, the SiO_2 -based glasses such as Ce-doped $\text{Li}_2\text{O}-\text{MgO}-\text{Al}_2\text{O}_3-\text{SiO}_2$ [23], Ce-doped SiO_2 [24], and Ce-doped $\text{Gd}_2\text{O}_3-\text{B}_2\text{O}_3-\text{Al}_2\text{O}_3-\text{SiO}_2$ [25] showed high light yields in the past reports. However, there are no reports on the radiation properties of $45\text{SrO}-5\text{Al}_2\text{O}_3-50\text{SiO}_2$ glasses. For these reasons, we have synthesized $45\text{SrO}-5\text{Al}_2\text{O}_3-50\text{SiO}_2$ glasses doped with various concentrations of Ce (0, 0.01, 0.05, 0.1, and 0.5 mol%) by the conventional melt-quenching method and examined the optical, scintillation, and TSL properties.

2 Experiment

$45\text{SrO}-5\text{Al}_2\text{O}_3-50\text{SiO}_2$ glasses doped with the different concentrations of Ce (0, 0.01, 0.05, 0.1, and 0.5 mol%) were synthesized by the conventional melt-quenching method. Raw powders of SrCO_3 ($\geq 99.9\%$, Kojundo Chemical Laboratory Co., Ltd.), Al_2O_3 ($\geq 99.99\%$, Kojundo Chemical Laboratory Co., Ltd.), SiO_2 ($\geq 99.999\%$, Kojundo Chemical Laboratory Co., Ltd.), and $\text{Ce}(\text{CH}_3\text{COO})_3 \cdot \text{H}_2\text{O}$ ($\geq 99.9\%$, Junsei Chemical Co., Ltd.) were mixed using a mortar and pestle. The mixtures were melted in the platinum crucible using an electric furnace at $1620\text{ }^\circ\text{C}$ for 30 min, and then the melts were quenched onto a stainless plate at $200\text{ }^\circ\text{C}$. The obtained glasses were eventually cooled to room temperature. In order to obtain thermal and structure stability, the glasses were annealed for 1 h at $750\text{ }^\circ\text{C}$. The obtained glasses were cut and polished to a mirror finish with CeO_2 powder. To evaluate the basic optical, scintillation, and TSL properties, the following measurements were carried out for all the obtained glasses.

The glass transition temperature (T_g) was determined by differential thermal analysis (DTA) operated at a heating rate of $10\text{ }^\circ\text{C}/\text{min}$ using TG8121 (Rigaku). Raman scattering spectra at room temperature were obtained using a laser Raman spectroscopy (JASCO Co., RMP-510; LD laser $\lambda = 532.172\text{ nm}$). In the optical properties, in-line transmittance spectra were obtained in the spectral range of 1902700 nm with 1 nm interval using a spectrophotometer (V670,

JASCO). Using Quantaurs-QY (C11347, Hamamatsu Photonics), the photoluminescence (PL) excitation/emission spectra and Quantum yield (QY) were measured. To obtain the PL decay curves, a Quantaurs- τ (C11367, Hamamatsu Photonics) was used. As the scintillation property, the X-ray-induced scintillation spectra were measured by our original setup [26]. During the measurement, the X-ray generator was operated with a supplied bias voltage and tube current of 40 kV and 1.2 mA , respectively. The X-ray-induced scintillation decay curves were measured by an X-ray-induced after-glow characterization system [27]. The excitation source was a pulse X-ray tube supplied with 30 kV bias voltage. To calculate the scintillation light yields, a pulse height spectra was measured using a laboratory-constructed setup which is explained elsewhere in detail [28]. Regarding the TSL properties, we evaluated TSL glow curves and TSL dose response function using a TSL reader (TL-2000, Nanogray Inc.) and an X-ray generator (XRB80P & N200 \times 4550, Spellman) [29, 30]. Series of TSL glow curves were measured with varying irradiation doses from 0.1 to 1000 mGy . During the measurements of TSL glow curve, the temperature range was 50 to $400\text{ }^\circ\text{C}$ and the heating rate was $1\text{ }^\circ\text{C}/\text{s}$.

3 Results and discussion

3.1 Samples

Figure 1 shows a photograph of non- and Ce-doped $\text{SrO}-\text{Al}_2\text{O}_3-\text{SiO}_2$ glasses under room light. The prepared glasses are placed in the ascending order of concentrations of Ce (0, 0.01, 0.05, 0.1, and 0.5 mol%) from left to right. In all the glasses, the area and thickness were fixed to approximately 1 cm^2 and 1.3 mm , respectively. Figure 2 indicates DTA curve of the non- and Ce-doped $\text{SrO}-\text{Al}_2\text{O}_3-\text{SiO}_2$ glasses. The T_g values of (0, 0.01, 0.05, 0.1, and 0.5%) Ce-doped glasses were 746 , 752 , 756 , 762 , and $765\text{ }^\circ\text{C}$,

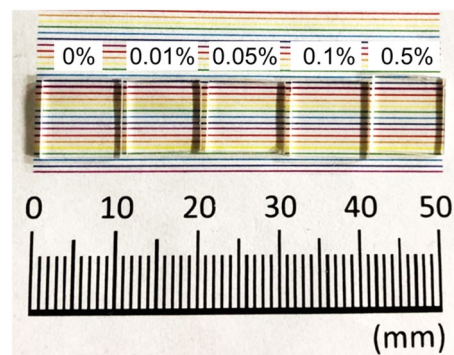


Fig. 1 Photographs of non- and Ce-doped $\text{SrO}-\text{Al}_2\text{O}_3-\text{SiO}_2$ glasses under room light. From left to right, the concentrations of Ce are 0, 0.01, 0.05, 0.1, and 0.5 mol%

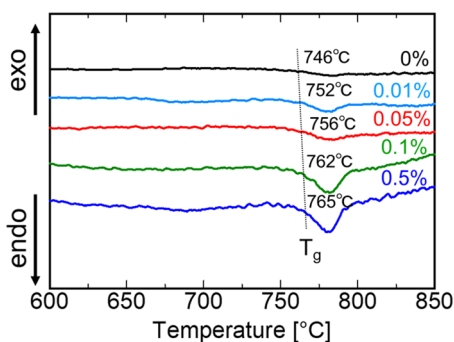


Fig. 2 DTA curve of the non- and Ce-doped SrO–Al₂O₃–SiO₂ glasses

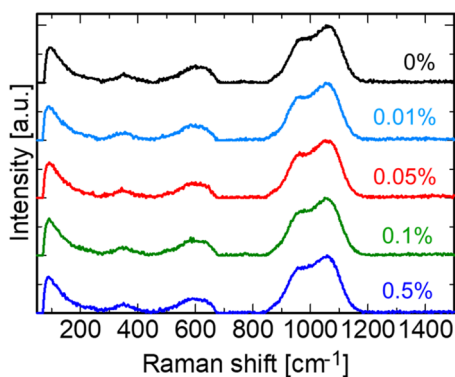


Fig. 3 Raman scattering spectra of the non- and Ce-doped SrO–Al₂O₃–SiO₂ glasses

respectively, and the T_g values were increased with increasing concentrations of Ce. The Raman scattering spectra of the non- and Ce-doped SrO–Al₂O₃–SiO₂ glass is shown Fig. 3. In all samples, multiple peaks appeared around 50, 350, 600, and 1000 cm^{-1} , and the obtained spectrum feature was similar to the past reports about SiO₂ glasses [31, 32]. The origin of low-frequency bands around 50 cm^{-1} was the boson peak which was an universal phenomenon in amorphous materials [31, 33]. At the mid-frequency band, the peak around 600 cm^{-1} arose from the symmetric stretching vibrations of some [AlO]_x species [32]. The high-frequency band around 1000 cm^{-1} was due to the optic-like Si–O–Si stretching vibrations of the tetrahedral SiO₄ unit [34].

3.2 Optical properties

Figure 4 shows the in-line transmittance spectra of non- and Ce-doped SrO–Al₂O₃–SiO₂ glasses. The transmittance of the glasses was ~90% in the spectral range of 400–2700 nm. In the non-doped glass, the calculated optical bandgap was ~5.59 eV [35]. In the Ce-doped glasses, an absorption band around 340 nm was observed, and it was a typical absorption

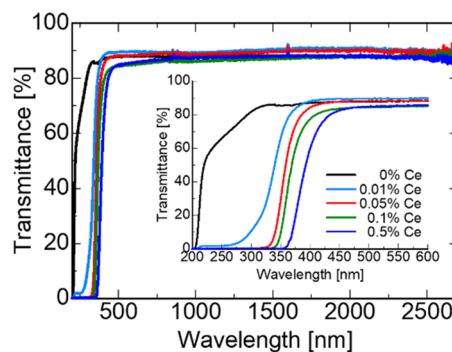


Fig. 4 In-line transmittance spectra of non- and Ce-doped SrO–Al₂O₃–SiO₂ glasses. The inset shows an enlarged view in the spectral range 200–600 nm

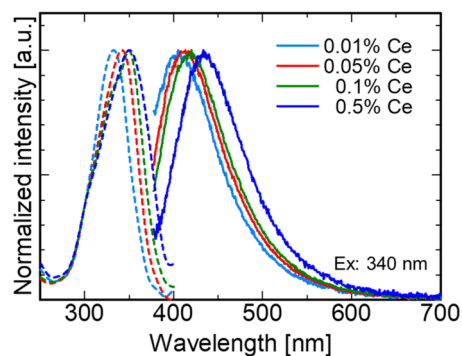


Fig. 5 PL excitation (dotted line) and emission (solid line) spectra of Ce-doped SrO–Al₂O₃–SiO₂ glasses

by the $4f \rightarrow 5d$ transitions of Ce^{3+} . The inset of Fig. 4 shows an enlarged view in the spectral range 200–600 nm. The optical absorption bands shifted to longer wavelengths as the Ce concentrations increased. PL excitation and emission spectra of the Ce-doped glasses are shown in Fig. 5. The non-doped glass did not show any measurable emission. The excitation spectra of the Ce-doped glasses were consistent with the absorptions due to the $4f \rightarrow 5d$ transitions of Ce^{3+} (shown in Fig. 4). Under an excitation of 340 nm \pm 20 nm, a broad emission band around 420 nm was observed. With increasing concentrations of Ce, the excitation and emission peak position shifted to longer wavelength side. The QYs of the glasses doped with the concentrations of Ce 0.01, 0.05, 0.1, and 0.5% were 13.4, 16.6, 15.9, and 8.3% with a typical error of $\pm 2\%$, respectively. Figure 6 indicates the PL decay curves of the Ce-doped glasses monitoring at 420 nm under an excitation (340 nm). The decay curves of the Ce-doped glasses were approximated by a single exponential decay function, and the decay constants of the glasses doped with concentrations of Ce 0.01, 0.05, 0.1, and 0.5% were 46.3, 46.7, 46.4, and 43.5 ns, respectively. From the excitation and emission spectra and PL decay constants, the

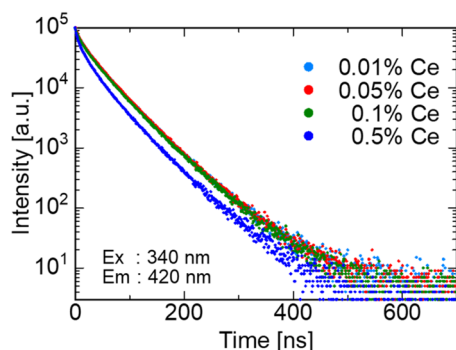


Fig. 6 PL decay curves of Ce-doped SrO–Al₂O₃–SiO₂ glasses monitoring at 420 nm under 340 nm excitation

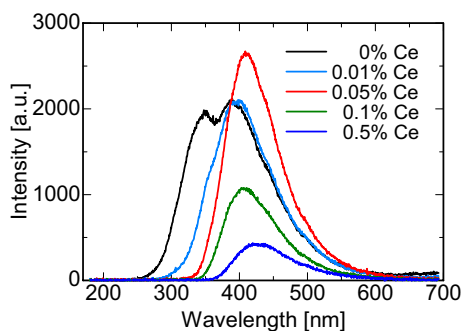


Fig. 7 X-ray-induced scintillation spectra of non- and Ce-doped SrO–Al₂O₃–SiO₂ glasses

origin of the emission around 420 nm was due to $5d \rightarrow 4f$ transitions of Ce^{3+} [36–38]. The QY and PL decay time constant decreased when the concentration of Ce exceeds 0.1%. These behaviors were considered as typical concentration quenching.

3.3 Scintillation and thermally stimulated luminescence (TSL) properties

Figure 7 indicates the X-ray-induced scintillation spectra of Ce-doped SrO–Al₂O₃–SiO₂ glasses. In the non-doped glass, the emission peaks appeared around 350 and 400 nm, while the Ce-doped glasses showed an emission peak around 400 nm. Regarding the Ce-doped glasses, the emission peak around 350 nm was not detected because of the absorptions due to the $4f \rightarrow 5d$ transitions of Ce^{3+} (as shown in Fig. 4). The origins of the emission were unclear because the emission of non- and Ce-doped glasses overlapped. The X-ray-induced scintillation decay curves of Ce-doped SrO–Al₂O₃–SiO₂ glasses are shown in Fig. 8. The scintillation decay curves of all the glasses were approximated by a sum of two exponential decay functions. The obtained decay time constants were around 0.14–0.24 μs (τ_1) and 1.96–2.24

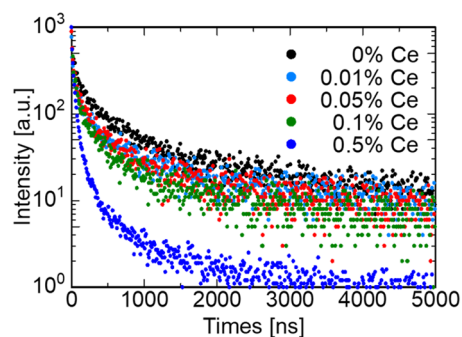


Fig. 8 X-ray-induced scintillation decay curves of non- and Ce-doped SrO–Al₂O₃–SiO₂ glasses

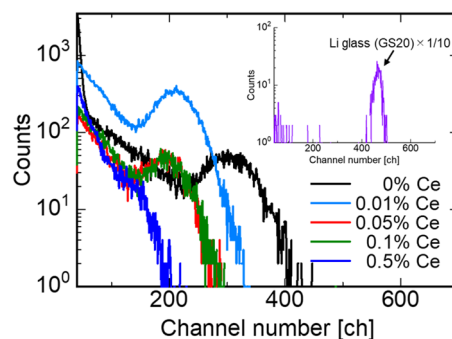


Fig. 9 Pulse height spectra of ^{241}Am α -ray measured using non- and Ce-doped SrO–Al₂O₃–SiO₂ glasses. The inset shows pulse height spectra of ^{252}Cf neutron measured using Li-glass scintillator (GS20) as a reference

μs (τ_2), as summarized in Table 1. In the non-doped glasses, from the results of emission peak and decay time constants, the emission peak around 350 and 400 nm would be due to some defects or impurity ions included in the host glass [39]. The scintillation decay time constants of the Ce-doped glasses were similar to that of non-doped glasses. In general, the decay time constant of the emission due to $5d \rightarrow 4f$ transitions of Ce^{3+} was several ten nanoseconds [36–38]. Therefore, we assign that the emission band of Ce-doped glasses are due to some defects or impurity ions included in the host glass.

Figure 9 shows the pulse height spectra of ^{241}Am α -ray (5.5 MeV) irradiation measured using non- and Ce-doped glasses. The commercial Li-glass scintillator (GS20, Saint-Gobain) was used as a reference (the inset of Fig. 9), which had the light yield of about 1255 photons/MeV under α -ray according to the previous report [40]. In all the glasses, the full energy peak of the glasses was confirmed, and the light yield of the glasses was calculated as listed in Table 2. Here, quantum efficiencies of the PMT for the spectral position were taken into consideration. Among the prepared glasses, the light yield of non-doped glass was the highest, which

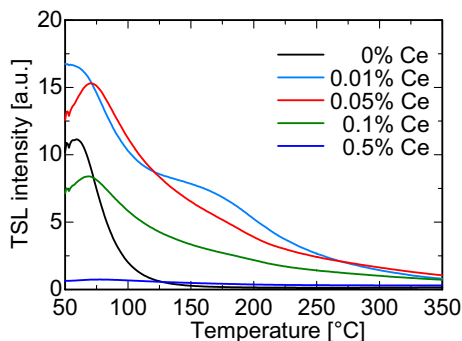


Fig. 10 TSL glow curves of non- and Ce-doped SrO–Al₂O₃–SiO₂ glasses measured after X-ray irradiation (100 mGy)

Table 1 X-ray-induced scintillation decay time constants of non- and Ce-doped SrO–Al₂O₃–SiO₂ glasses

Ce concentration (%)	X-ray induced scintillation decay time constants	
	τ_1 (μ s)	τ_2 (μ s)
0	0.29	2.24
0.01	0.25	2.20
0.05	0.24	2.14
0.1	0.23	2.14
0.5	0.14	1.96

Table 2 The peak position and calculated light yield from pulse height spectra of non- and Ce-doped glass under ²⁴¹Am α -ray (5.5 MeV)

Samples	Full energy peak position (ch)	Light yield (photons/MeV)
Non-doped glass	300	69
0.01% Ce-doped glass	207	50
0.05% Ce-doped glass	189	47
0.1% Ce-doped glass	189	47
0.5% Ce-doped glass	106	27

was 69 photons/MeV with a typical error of $\pm 10\%$. When the concentrations of Ce were increasing, the light yield of the glasses was decreasing. This is the first report on the light yield of non- and Ce-doped SrO–Al₂O₃–SiO₂ glasses although the light yield of the non-doped glasses was 10 times as low as GS20.

Figure 10 presents TSL glow curves of non- and Ce-doped SrO–Al₂O₃–SiO₂ glasses measured after X-ray irradiation (100 mGy). The non-doped glass showed a major peak around 80 °C, and the glow peak feature was similar to the past report about Sr-containing glasses [41, 42]. The Ce-doped glasses showed two glow peaks around 80 and

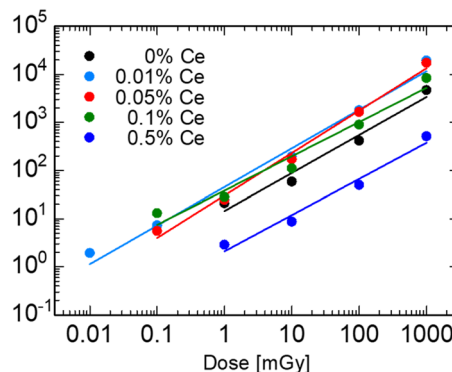


Fig. 11 TSL dose response curves of non- and Ce-doped SrO–Al₂O₃–SiO₂ glasses from 0.01 to 1000 mGy

170 °C, and the TSL intensity of 0.01% Ce-doped glass was the highest among the prepared glasses. Since the peak features were different between non- and Ce-doped glasses, we assume that the TSL glow peaks around 170 °C would be related to doped Ce. Figure 11 shows a relationship between the TSL intensity and irradiated X-ray dose, namely the TSL dose response function. Here, the TSL intensity was defined as an integrated signal from 50 to 350 °C. The 0.01% Ce-doped glass showed a good linearity from 0.01 to 1000 mGy.

In the previous reports, the scintillation light yield and TSL intensity were related complementarily in some material [8–12]. However, in this material, the relationship between scintillation light yield and TSL intensity was not observed. As a possible reason, the stored energy was released by stimulation at room temperature because the TSL glow peak position of the glasses was at relatively low temperature. The duration after X-rays irradiation and setting the sample in the TSL reader requires several minutes, and carriers at shallow traps would be released within this time lag. Thus, in this material, discussing the relationship between scintillation light yields and TSL intensity is difficult.

4 Conclusion

45SrO–5Al₂O₃–50SiO₂ glasses with various concentrations of Ce (0, 0.01, 0.05, 0.1, and 0.5 mol%) were synthesized by the conventional melt-quenching method, and the basic optical, scintillation, and TSL properties were evaluated. In the Raman scattering spectra, the obtained spectrum feature was similar to the previous report about SiO₂ glass. The transmittance of the glasses was $\sim 90\%$ in the spectral range 400–2700 nm. Under an excitation (340 nm \pm 20 nm), a broad emission band around 420 nm was observed in the Ce-doped glasses, and the origin of the emission was the 5d \rightarrow 4f transitions of Ce³⁺. In contrast, X-ray-induced

scintillation spectra of all the glasses showed a broad emission peak around 400 nm, and the emission band of Ce-doped glasses were due to some defects or impurity ions included in the host glass. In the pulse height spectra, the full energy peak of the non-doped glass was confirmed, and the calculated light yield for α -ray was 69 photons/MeV with a typical error of $\pm 10\%$. As TSL properties, the TSL glow curves of Ce-doped glasses showed two glow peaks around 80 and 170 °C. The TSL intensity of 0.01% Ce-doped glass was the highest among the prepared glasses, and the lowest detectable sensitivity was 0.01 mGy.

Acknowledgements This work was supported by Grant-in-Aid for Scientific Research A (Grant No. 17H01375), Scientific Research B (Grant No. 18H03468), and JSPS Fellows (Grant No. 19J22091) from JSPS. The Cooperative Research Project of Research Institute of Electronics, Shizuoka University, Murata Foundation, Iketani Foundation, Nippon Sheet Glass Foundation, and NAIST foundation are also acknowledged.

References

1. C.W.E. van Eijk, Nucl. Instrum. Methods Phys. Res. Sect. A **509**, 17 (2003)
2. H. Nanto, A. Nishimura, M. Kuroda, Y. Takei, Y. Nakano, T. Shoji, T. Yanagita, S. Kasai, Nucl. Instrum. Methods Phys. Res. Sect. A **580**, 278 (2007)
3. N.M. Winch, A. Edgar, C.M. Bartle, Nucl. Instrum. Methods Phys. Res. Sect. A **763**, 394 (2014)
4. J.M. Hall, S. Asztalos, P. Bilotft, J. Church, M.A. Descalle, T. Luu, D. Manatt, G. Mauger, E. Norman, D. Petersen, J. Pruet, S. Prussin, D. Slaughter, Nucl. Instrum. Methods Phys. Res. Sect. B **261**, 337 (2007)
5. R.W. Christy, N.M. Johnson, R.R. Wilbarg, J. Appl. Phys. **38**, 2099 (1967)
6. Y. Tsubota, J.H. Kaneko, M. Higuchi, S. Nishiyama, H. Ishibashi, Appl. Phys. Express **8**, 6 (2015)
7. T. Itoh, T. Yanagida, M. Kokubun, M. Sato, Nucl. Instrum. Methods Phys. Res. Sect. A **579**, 239 (2007)
8. T. Yanagida, J. Lumin. **169**, 544 (2016)
9. T. Yanagida, G. Okada, N. Kawaguchi, J. Lumin. **207**, 14 (2019)
10. T. Yanagida, Proc. Jpn. Acad. Ser. B **94**, 75–97 (2018)
11. H. Kimura, T. Kato, D. Nakauchi, G. Okada, N. Kawaguchi, T. Yanagida, Nucl. Instrum. Methods Phys. Res. Sect. A. <https://doi.org/10.1016/j.nima.2018.09.061> (2018)
12. H. Kimura, F. Nakamura, T. Kato, D. Nakauchi, N. Kawano, G. Okada, N. Kawaguchi, T. Yanagida, Optik **157**, 421 (2018)
13. C.W.E. van Eijk, Nucl. Instrum. Methods Phys. Res. Sect. A. **460**, 1 (2001)
14. T. Yanagida, Y. Fujimoto, M. Koshimizu, K. Watanabe, H. Sato, H. Yagi, T. Yanagitani, Opt. Mater. **36**, 2016 (2014)
15. H. Masai, T. Yanagida, J. Non. Cryst. Solids **431**, 83 (2016)
16. T. Kuro, G. Okada, N. Kawaguchi, Y. Fujimoto, H. Masai, Opt. Mater. **62**, 561 (2016)
17. Y. Fujimoto, T. Yanagida, M. Koshimizu, K. Asai, J. Ceram. Soc. Jpn. **125**, 728 (2017)
18. A. Torimoto, H. Masai, G. Okada, N. Kawaguchi, T. Yanagida, Opt. Mater. **73**, 517 (2017)
19. H. Nanto, R. Nakagawa, Y. Takei, K. Hirasawa, Y. Miyamoto, H. Masai, T. Kurobori, T. Yanagida, Y. Fujimoto, Nucl. Instrum. Methods Phys. Res. Sect. A. **784**, 14 (2015)
20. Y. Oshima, T. Yasumune, T. Masuda, K. Maehata, K. Ishibashi, T. Umeno, Prog. Nucl. Sci. Technol. **1**, 296 (2011)
21. A. Rupesh Kumar, T.G.V.M. Rao, N. Veeraiah, M. Rami, Reddy, Opt. Mater. **35**, 402 (2013)
22. H. Li, L. Liu, X. Tang, Q. Wang, P.W. Wang, Glas. Phys. Chem. **43**, 548 (2017)
23. T. Yanagida, J. Ueda, H. Masai, Y. Fujimoto, S. Tanabe, J. Non. Cryst. Solids **431**, 140 (2016)
24. Y. Isokawa, H. Kimura, T. Kato, N. Kawaguchi, T. Yanagida, Opt. Mater. **90**, 187 (2019)
25. W. Chewpraditkul, X. He, D. Chen, Y. Shen, Q. Sheng, B. Yu, M. Nikl, R. Kucerkova, A. Beitlerova, C. Wanarak, A. Phunpueok, Phys. Status Solidi Appl. Mater. Sci. **208**, 2830 (2011)
26. T. Yanagida, K. Kamada, Y. Fujimoto, H. Yagi, T. Yanagitani, Opt. Mater. **35**, 2480 (2013)
27. T. Yanagida, Y. Fujimoto, T. Ito, K. Uchiyama, K. Mori, Appl. Phys. Express **7**, 062401 (2014)
28. H. Kimura, F. Nakamura, T. Kato, D. Nakauchi, G. Okada, N. Kawaguchi, T. Yanagida, J. Mater. Sci. Mater. Electron. **29**, 8498 (2018)
29. T. Yanagida, Y. Fujimoto, N. Kawaguchi, S. Yanagida, J. Ceram. Soc. Japan **121**, 988 (2013)
30. H. Kimura, T. Kato, D. Nakauchi, M. Koshimizu, N. Kawaguchi, T. Yanagida, Sensors Mater **30**, 1 (2018)
31. M. Ivanda, R. Clasen, M. Hornfeck, W. Kiefer, J. Non. Cryst. Solids **322**, 46 (2003)
32. M. Okuno, N. Zotov, M. Schmücker, H. Schneider, J. Non. Cryst. Solids **351**, 1032 (2005)
33. Y. Isokawa, S. Hirano, N. Kawano, G. Okada, N. Kawaguchi, T. Yanagida, Opt. Mater. **76**, 28 (2018)
34. N. Zotov, I. Ebbsjö, D. Timpel, H. Keppeler, Phys. Rev. B **60**, 6383 (1999)
35. A.M. Abd-Elnaiem, M. Mohamed, R.M. Hassan, A.A. Abu-Sehly, M.A. Abdel-Rahim, M.M. Hafiz, Mater. Sci. **35**, 335 (2017)
36. H. Kimura, F. Nakamura, T. Kato, D. Nakauchi, G. Okada, N. Kawaguchi, T. Yanagida, Sensors Mater. **30**, 1555 (2018)
37. U. Caldiño, J.L. Hernández-Pozos, C. Flores, A. Speghini, M. Bettinelli, J. Phys. Condens. Matter **17**, 7297 (2005)
38. Y. Fujimoto, T. Yanagida, Y. Futami, H. Masai, Jpn. J. Appl. Phys. **53**, 05FK05 (2014)
39. L. Skuja, J. Alloys Compd. **239**, 16 (1996)
40. M. Akatsuka, K. Shinozaki, D. Nakauchi, T. Kato, G. Okada, N. Kawaguchi, T. Yanagida, Opt. Mater. **94**, 86 (2019)
41. N. Kawano, N. Kawaguchi, G. Okada, Y. Fujimoto, T. Yanagida, J. Non. Cryst. Solids **482**, 154 (2018)
42. H. Kimura, K. Shinozaki, G. Okada, N. Kawaguchi, T. Yanagida, J. Non. Cryst. Solids **508**, 46 (2018)

Publisher's Note Springer Nature remains neutral with regard to jurisdictional claims in published maps and institutional affiliations.